

PQCAD-DM: Progressive Quantization and Calibration-Assisted Distillation for Extremely Efficient Diffusion Model

Beomseok Ko, *Student Member, IEEE*, and Hyeryung Jang, *Member, IEEE*

Abstract—Diffusion models excel in image generation but are computational and resource-intensive due to their reliance on iterative Markov chain processes, leading to error accumulation and limiting the effectiveness of naive compression techniques. In this paper, we propose PQCAD-DM, a novel hybrid compression framework combining Progressive Quantization (PQ) and Calibration-Assisted Distillation (CAD) to address these challenges. PQ employs a two-stage quantization with adaptive bit-width transitions guided by a momentum-based mechanism, reducing excessive weight perturbations in low-precision. CAD leverages full-precision calibration datasets during distillation, enabling the student to match full-precision performance even with a quantized teacher. As a result, PQCAD-DM achieves a balance between computational efficiency and generative quality, halving inference time while maintaining competitive performance. Extensive experiments validate PQCAD-DM’s superior generative capabilities and efficiency across diverse datasets, outperforming fixed-bit quantization methods.

Index Terms—Diffusion Models, Quantization, Distillation, Model Compression

I. INTRODUCTION

DIFFUSION models (DMs) [1] have emerged as a foundational technology for generative tasks, producing high-quality images with a balance of diversity and fidelity. They address issues such as mode collapse in GANs [2], [3] and blur artifacts in VAEs [4], making them highly effective for tasks ranging from image inpainting [5], [6] to graph generation [7] and molecular modeling [8]. However, the iterative generation process of DMs requires a large number of sampling steps, resulting in significant computational demands and slower inference speeds compared to other generative models. For instance, training state-of-the-art DMs can require hundreds of GPU days (e.g., 150-1000 days on V100 in [3]), making deployment challenging. This limits their practicality in resource-constrained environments, such as edge devices or real-time applications.

This research was supported by the MSIT(Ministry of Science and ICT), Korea, under the ITRC(Information Technology Research Center) support program(IITP-2025-2020-0-01789), and the Artificial Intelligence Convergence Innovation Human Resources Development(IITP-2025-RS-2023-00254592) supervised by the IITP(Institute for Information & Communications Technology Planning & Evaluation). *The first two authors contributed equally to this work.*

Beomseok Ko and Hyeryung Jang are with the Department of Computer Science & Artificial Intelligence, Dongguk University, Seoul, South Korea (Corresponding Author: Hyeryung Jang) (emails: {roy7001, hyeryung.jang}@dgu.ac.kr)

Recent efforts have explored quantization and distillation to alleviate these computational challenges in two directions: reducing model size and accelerating sampling time. Quantization reduces the bit-width of weights and activations, lowering memory and computational costs, with Post-Training Quantization (PTQ) being particularly useful in diffusion models as it compresses models without requiring retraining [9], [10]. At the same time, distillation transfers knowledge from a large teacher model to a smaller student model, accelerating sampling speed [11], [12]. Despite these advancements, combining these techniques effectively for diffusion models remains underexplored. Quantization can lead to cumulative errors, especially in iterative processes in DMs, and the sequence of applying distillation and quantization critically impacts performance if not carefully managed, as illustrated in Fig. 1.

In this paper, we propose PQCAD-DM, a hybrid compression framework that combines Progressive Quantization and Calibration-Assisted Distillation to reduce the computational complexity of diffusion models. The core features of PQCAD-DM include: (i) Progressive Quantization (PQ) that employs variable bit-widths to precisely control excessive weight perturbations at low bit precision, addressing the temporal variability in DMs with time-aware calibration datasets; and (ii) Calibration-Assisted Distillation (CAD) that mitigates inaccuracies inherited from the quantized teacher model during distillation by using a full-precision calibration dataset, ensuring minimal degradation in student model performance. This unified approach enhances quantization accuracy, prevents performance degradation during subsequent distillation, and strikes a balance between model quality and computational efficiency, achieving both high generative quality and improved inference speed.

Our contributions are summarized as follows:

- We propose PQCAD-DM, a hybrid compression framework that integrates progressive quantization and calibration-assisted distillation. This approach reduces model size and sampling steps, enabling faster inference while preserving the performance and generative quality of diffusion models.
- We introduce a progressive quantization strategy to minimize weight disturbances at low precision and incorporate full-precision calibration during distillation, effectively balancing the computational efficiency and generative accuracy of the final compressed DMs.
- Extensive experiments on CIFAR-10, ImageNet, CelebA-

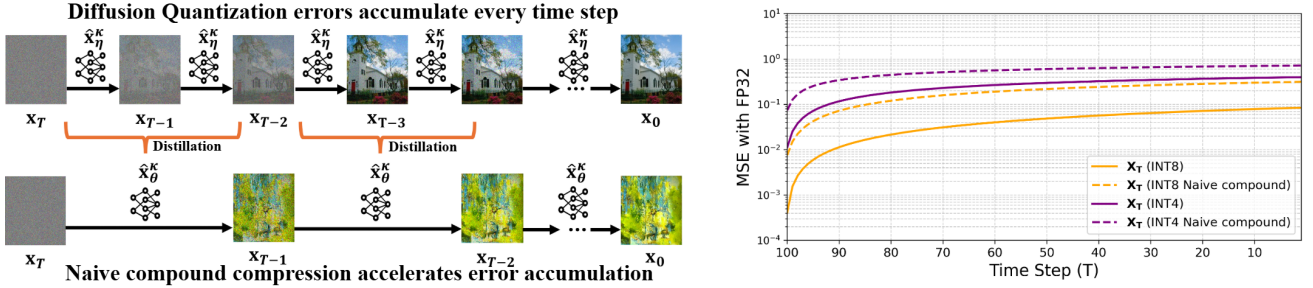


Fig. 1: (Left) Compounding quantization and distillation in DMs introduces cumulative errors at each time step, significantly impacting generative performance. (Right) Mean squared error (MSE) comparisons between the full-precision DDIM (100-time step ImageNet-trained) and both PTQ4DM quantized and naive compounded models highlight the need to mitigate error propagation during compression.

HQ, and LSUN-Bedrooms/Churches datasets demonstrate that PQCAD-DM achieves competitive image quality (regarding FID, sFID, and IS) while significantly reducing computational overhead, halving inference time and improving FID by 0.17 on average compared to quantization baseline methods.

II. RELATED WORKS

Efficient Diffusion Models. Various approaches have been studied to improve the efficiency of diffusion models (DMs), including optimized sampling [?], [13], [14], [15], [16], pruning [17], [18], parameter quantization [9], [10], and knowledge distillation [11], [19]. Sampling methods like DDIM reduce generation time at the cost of resources and time for training, while pruning and post-training quantization (PTQ) methods reduce the model size and memory consumption without re-training. Distillation accelerates DM sampling by transferring knowledge from a teacher model (with long sampling steps) to a student model (with shorter steps). Despite their individual strengths, these approaches often focus on a single aspect of compression, such as sampling or quantization, and fail to address the cumulative errors that arise when combining compression methods.

Progressive Quantization. Low-precision quantization introduces significant challenges during training due to quantization noise, prompting the development of progressive quantization techniques. These methods gradually reduce precision (or bit-widths), starting with high precision and transitioning to lower bit-widths [20], [21], [22], [23], [24], [25]. For instance, strategies like bit-shrinking [25] adaptively transition bit-widths, enabling simultaneous quantization of weights and activations with minimum errors. While effective in traditional networks, their application to DMs is limited due to the temporal variability of activations inherent in the diffusion process, requiring specialized strategies, such as time-aware calibration, to effectively manage the unique challenges posed by DM quantization.

III. PRELIMINARY

Diffusion Models. Diffusion models (DMs) [13], [26] generate data (e.g., images) through a forward and reverse process (see Fig. 1). In the forward process, Gaussian noise $\epsilon \sim \mathcal{N}(\mathbf{0}, \mathbf{I})$ is gradually added to input data $\mathbf{x} \sim p_{\text{data}}(\mathbf{x})$

over T time steps, transforming it into a noisy version $\{\mathbf{x}_0 = \mathbf{x}, \mathbf{x}_1, \dots, \mathbf{x}_T\}$. The reverse process removes the noise to reconstruct the original data. Given noise ϵ and noise schedule factors $\{\alpha_t, \sigma_t\}_{t=0}^T$, the DM \hat{x}_η (with trainable parameters η) takes $\mathbf{z}_t = \alpha_t \mathbf{x} + \sigma_t \epsilon$ as input and is trained by minimizing the weighted mean squared error between the original data \mathbf{x} and the denoised output $\hat{x}_\eta(\mathbf{z}_t)$:

$$\mathcal{L}_{\text{DM}} = \mathbb{E}_{t, \mathbf{x} \sim p_{\text{data}}(\mathbf{x}), \mathbf{z}_t \sim q(\mathbf{z}_t | \mathbf{x})} \left[w(\lambda_t) \|\mathbf{x} - \hat{x}_\eta(\mathbf{z}_t)\|_2^2 \right], \quad (1)$$

where $t \sim \text{U}[0, 1]$ is (normalized) time-step; $q(\mathbf{z}_t | \mathbf{x}) = \mathcal{N}(\mathbf{z}_t; \alpha_t \mathbf{x}, \sigma_t^2 \mathbf{I})$; $\lambda_t = \log(\alpha_t^2 / \sigma_t^2)$ denotes the signal-to-noise ratio (SNR); and $w(\cdot)$ is a pre-defined weight function. After training, the reverse process is efficiently handled by the discrete-time DDIM [14] sampler, which updates \mathbf{z}_s using the model's predictions at each step $s \in [0, 1]$. Starting from $\mathbf{z}_t \sim \mathcal{N}(\mathbf{0}, \mathbf{I})$, the updates are given by:

$$\mathbf{z}_s = \alpha_s \hat{x}_\eta(\mathbf{z}_t) + \sigma_s \left(\frac{\mathbf{z}_t - \alpha_s \hat{x}_\eta(\mathbf{z}_t)}{\sigma_t} \right), \quad \text{for } s = t - 1/T. \quad (2)$$

Distillation of Diffusion. Distillation techniques for diffusion models [11], [12] aim to reduce the number of sampling steps required in the reverse process, accelerating inference. The student model \hat{x}_θ (with trainable parameters θ) is trained to align one of its steps with two steps performed by the teacher model \hat{x}_η , effectively halving the required sampling steps from T to $T/2$. The teacher performs two DDIM sampling steps, first from t to $t' = t - 0.5/T$, and then from t' to $t'' = t - 1/T$. Instead of targeting the original data \mathbf{x} as in (2), the student learns to match the teacher's outcome of these two steps using a single step. The intermediate updates for the teacher are given by:

$$\begin{aligned} \mathbf{z}_{t'} &= \alpha_{t'} \hat{x}_\eta(\mathbf{z}_t) + \frac{\sigma_{t'}}{\sigma_t} (\mathbf{z}_t - \alpha_t \hat{x}_\eta(\mathbf{z}_t)), \\ \mathbf{z}_{t''} &= \alpha_{t''} \hat{x}_\eta(\mathbf{z}_{t'}) + \frac{\sigma_{t''}}{\sigma_{t'}} (\mathbf{z}_{t'} - \alpha_{t'} \hat{x}_\eta(\mathbf{z}_{t'})). \end{aligned}$$

The target $\tilde{\mathbf{x}}$ for the student is then computed as $\tilde{\mathbf{x}} = \frac{\mathbf{z}_{t''} - (\sigma_{t''}/\sigma_t) \mathbf{z}_t}{\alpha_{t''} - (\sigma_{t''}/\sigma_t) \alpha_t}$. Using this target, the objective for student model \hat{x}_θ is modified to:

$$\mathcal{L}_{\text{Dist}} = \mathbb{E}_{t, \mathbf{x} \sim p_{\text{data}}(\mathbf{x}), \mathbf{z}_t \sim q(\mathbf{z}_t | \mathbf{x})} \left[w(\lambda_t) \|\tilde{\mathbf{x}} - \hat{x}_\theta(\mathbf{z}_t)\|_2^2 \right]. \quad (3)$$

Post-Training Quantization (PTQ) of Diffusion. In diffusion models (DMs), the activation distribution of the noise estimation network varies significantly across time steps, as each step

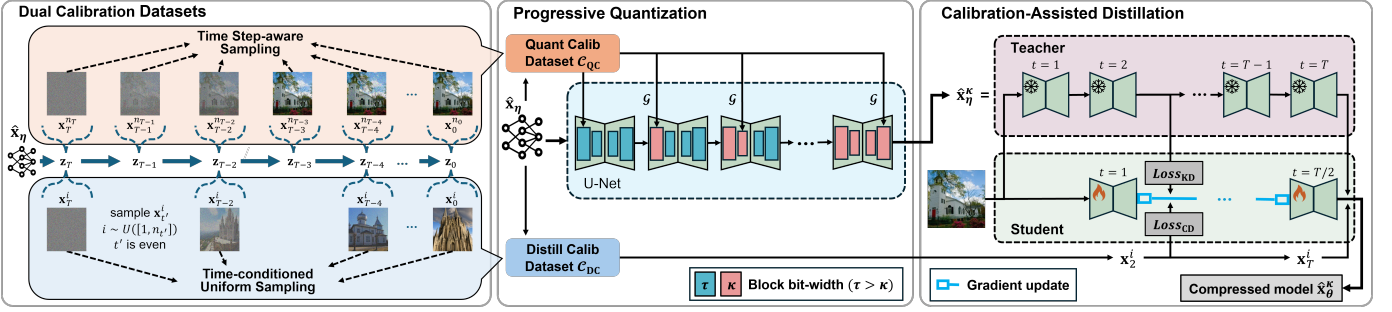


Fig. 2: Overview of PQCAD-DM framework. (Left) Dual calibration datasets, (Center) Progressive Quantization (PQ), and (Right) Calibration-Assisted Distillation (CAD) optimize compression and generative quality.

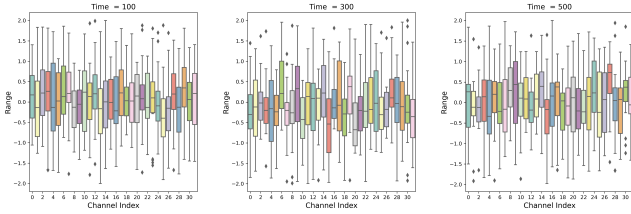


Fig. 3: Activation distribution over time step of diffusion. Figure shows the outputs of the first attention block of a DDIM model pre-trained on the CIFAR-10 dataset, presented using boxplots for each time step. A boxplot represents the median, max, and min values.

takes the output of the previous one as input. This temporal dependency causes the same network to exhibit drastically different activation patterns over time (Fig. 3), particularly in deeper layers. As a result, PTQ in diffusion models (DMs) faces significant challenges due to activation variability across time steps. Recent methods [9], [10], [27], [?], [?], [28] address this issue by constructing *time-step-specific* calibration datasets that capture activation and weight distributions at each step, ensuring stable performance in quantized models. Q-Diff [10] uses residual bottleneck and transformer blocks for reconstruction, calibrating weight quantizers and employing layer-wise reconstruction and split quantization to preserve UNet performance. PTQ4DM [9] enhances this with block-wise reconstruction and introduces QDrop, a mechanism that randomly skips activation quantization to exploit model flatness. TFMQ-DM [28] refines Q-Diff by addressing calibration overfitting and temporal feature variability with a temporal-aware reconstruction process. All methods maintain generative quality by prescaling weights during quantization and applying activation quantization to handle variability.

Low-bit Post-Training Quantization. Reconstruction-based quantization methods [29], [30] learn to adjust weights by rounding up or down, modeling the rounding operation as weight perturbation ($\hat{\eta} = \eta + \Delta\eta$). For a pre-trained DM with weights η , these methods analyze the quantization objective, with $\hat{\eta}$ being quantized weights, using a Taylor expansion to capture the interactions between weights. The objective is expressed as:

$$\min_{\hat{\eta}} \mathbb{E} \left[\hat{\mathbf{x}}_{\hat{\eta}}(\mathbf{z}_t) - \hat{\mathbf{x}}_{\eta}(\mathbf{z}_t) \right] \approx \mathbb{E} \left[\frac{1}{2} \Delta\eta^{\top} \mathbf{H}^{\eta} \Delta\eta \right], \quad (4)$$

where $\mathbf{H}^{\eta} = \mathbb{E} \nabla_{\eta}^2 \hat{\mathbf{x}}_{\eta}(\mathbf{z}_t)$ represents the expected Hessian of

the output with respect to the weights η . This reformulation shows that the quantization objective depends on the change in weights, scaled by the output Hessian. The objective can further be approximated at the block or layer level:

$$\min_{\hat{\eta}} \mathbb{E} \left[\Delta\eta^{\top} \mathbf{H}^{\eta} \Delta\eta \right] \approx \mathbb{E} \left[\Delta\mathbf{a}^{\top} \mathbf{H}^{\mathbf{a}} \Delta\mathbf{a} \right], \quad (5)$$

where \mathbf{a} represents the output of a layer or block. By refining weights to minimize the error between quantized and full-precision outputs at the block level, these methods better address inter-layer dependencies and generalization compared to fully layer-wise corrections. This block-wise reconstruction improves overall performance, effectively balancing quantization noise and accuracy.

IV. METHOD

A. PQCAD-DM: Overall Framework

PQCAD-DM is a hybrid compression framework designed to reduce the computational overhead of diffusion models in terms of time, energy, and memory, without significant performance degradation. It integrates two key components:

- 1) **Progressive Quantization (PQ):** PQ gradually reduces model bit-widths in stages to minimize quantization-induced errors. A momentum-based bit transition mechanism is employed for precise control of weight and activation quantization.
- 2) **Calibration-Assisted Distillation (CAD):** CAD mitigates inaccuracies inherited from quantized teacher models by utilizing a high-quality calibration dataset, allowing the student model to maintain efficiency and accuracy in the inference process.

As illustrated in Fig. 2, PQCAD-DM sequentially applies these techniques, reducing both model size and sampling steps. In the PQ phase, the pre-trained diffusion model $\hat{\mathbf{x}}_{\eta}$ is first quantized to τ -bit precision, producing $\hat{\mathbf{x}}_{\eta}^{\tau}$. A second stage of quantization further reduces the precision of weights and activations to κ -bits, yielding $\hat{\mathbf{x}}_{\eta}^{\kappa}$. In the CAD phase, the κ -bit teacher model with T sampling steps is distilled to produce the student model $\hat{\mathbf{x}}_{\theta}^{\kappa}$, which requires only $T/2$ inference steps. This sequential approach ensures that errors introduced during quantization are mitigated before distillation, achieving a trade-off between computational efficiency and generative quality.

B. Dual Calibration Datasets

As shown in Fig. 2 (left), PQCAD-DM employs two distinct calibration datasets to ensure accurate quantization and effective distillation.

Quantization Calibration Dataset. In DMs, activation distributions vary significantly across time steps, necessitating a calibration dataset that reflects these variations. \mathcal{C}_{QC} is constructed using a *time step-aware sampling* method that captures the input distribution at arbitrary time steps, tailored to each baseline quantization method. First, PTQ4DM [9] collects calibration data from a pre-trained full-precision (FP) model $\hat{\mathbf{x}}_\eta$ by using a Normally Distributed Time-step Calibration (NDTC) strategy, sampling n_t images per time step t with a Gaussian distribution centered on mid-time intervals to minimize degradation. In contrast, Q-Diffusion [10] and TFMQ-DM [28] employ uniform sampling across all time steps ($n_t = n_{\text{fixed}}$), maintaining a balance between dataset size and representational capacity. PQCAD-DM adapts these time step-aware sampling strategies, constructing \mathcal{C}_{QC} to reflect the input distribution required for effective quantization while accommodating the characteristics of the base FP model.

Distillation Calibration Dataset. Distillation in PQCAD-DM utilizes a calibration dataset \mathcal{C}_{DC} tailored to the student model, which has halved sampling steps compared to the quantized teacher model. To match this reduced step count, \mathcal{C}_{DC} is created using the full-precision (FP) model $\hat{\mathbf{x}}_\eta$, which provides a high-capacity reference for guiding the student model during distillation. This approach is especially critical when the teacher model is quantized, as the quantized teacher may lack sufficient capacity to effectively guide the student under traditional distillation methods. As shown in Fig. 2 (left), calibration data is generated at even time steps (e.g., $2, 4, \dots, T$) from the FP model with noise intensities closely matching those at the corresponding inference steps of the student model (e.g., $1, 2, \dots, T/2$), thus we call it *time-conditioned uniform sampling*. To introduce variability and avoid overfitting, random noise is applied at each step to generate stochastic, diverse outputs ($\mathcal{C}_{\text{DC}} \leftarrow \mathcal{C}_{\text{DC}} \cup \{\mathbf{x}_t^i\}$, where $i \sim \mathcal{U}([1, n_t])$) at every step. By leveraging the FP model’s stochastic outputs, \mathcal{C}_{DC} enables the student model to retain the generative quality and precision of the FP model, effectively mitigating limitations introduced by the quantized teacher. Details about \mathcal{C}_{DC} construction are provided in the Alg. 1

C. Progressive Quantization (PQ)

Quantizing DMs presents unique challenges, particularly at low precision (e.g., 4-bit), where weight perturbations can lead to significant quantization noise [25]. Previous approaches [9], [10], [28] primarily employed block or layer-wise reconstruction [30], [29] to minimize this noise, which proved effective for small calibration datasets and inter-layer dependencies but struggled with severe perturbations at lower precision levels.

Two-stage Quantization. To address this, our *Progressive Quantization (PQ)* framework follows a two-stage process to minimize errors during low-bit quantization. The first stage reduces the precision of a full-precision model $\hat{\mathbf{x}}_\eta$ to an intermediate bit-width τ to minimize early perturbations.

Algorithm 1 Calibration Dataset Collection

- 1: **Input:** Pre-trained diffusion model $\hat{\mathbf{x}}_\eta$, calibration datasets $\mathcal{C}_{\text{QC}}, \mathcal{C}_{\text{DC}}$, total sampling steps T , mean of the Normal distribution μ ,
- 2: **Output:** Calibration datasets $\mathcal{C}_{\text{QC}}, \mathcal{C}_{\text{DC}}$

- 3: Initialize $\mathcal{C}_{\text{QC}} = \emptyset, \mathcal{C}_{\text{DC}} = \emptyset$
- 4: **for** $t = 1, \dots, T$ **do**
- 5: Sample n_{max} intermediate inputs $\mathbf{x}_t^1, \dots, \mathbf{x}_t^{\text{max}}$ from $\hat{\mathbf{x}}_\eta(\mathbf{z}_t^{n_{\text{max}}})$
- 6: Determine n_t as follows:

$$n_t = \begin{cases} n_t \sim \mathcal{N}(\mu, T/2), & \text{if PTQ4DM,} \\ n_{\text{fixed}}, & \text{else otherwise} \end{cases}$$
- 7: Update $\mathcal{C}_{\text{QC}} \leftarrow \mathcal{C}_{\text{QC}} \cup \{\mathbf{x}_t^1, \dots, \mathbf{x}_t^{n_t}\}$
- 8: **if** $t \bmod 2 = 0$ **then** ▷ For distill calibration data
- 9: Update $\mathcal{C}_{\text{DC}} \leftarrow \mathcal{C}_{\text{DC}} \cup \{\mathbf{x}_t^i\}$, where $i \sim \text{Uniform}([1, n_t])$
- 10: **end if**
- 11: **end for**

In the second stage, the τ -bit model $\hat{\mathbf{x}}_\eta^\tau$ undergoes further quantization to the target precision κ , producing the model $\hat{\mathbf{x}}_\eta^\kappa$. During init quantization, the scaling factors and clipping range of the weight quantizer \mathcal{Q} are set for an intermediate bit-width τ , which is often chosen to be double the target bit-width κ (i.e., $\tau = 2\kappa$) for better memory alignment and efficient processing [20].

As described in Alg. 2, for each block or layer i , the calibration outputs $\hat{\mathbf{a}}_i \in \mathcal{C}_{\text{QC}}$ are quantized to a desirable bit-width b (either τ or κ) using the quantizer \mathcal{Q} : $\mathbf{a}_i^b := \mathcal{Q}(\hat{\mathbf{a}}_i, b)$. Then, the perturbation $\hat{\mathbf{a}}_i$ is computed (line 9), then used to minimize the objective (5). The quantized model weights η_i^b are iteratively refined by using the gradient update:

$$\eta_i^b \leftarrow \eta_i^b - \gamma \nabla_{\eta_i^b} \mathbb{E} \left[\Delta \mathbf{a}_i^\top \mathbf{H}^{\mathbf{a}_i} \Delta \mathbf{a}_i \right], \quad (6)$$

where γ is the learning rate. This update step is repeated to ensure the quantized weights align closely with the FP model, reducing reconstruction errors. Unlike weight quantization, activation quantization is more challenging due to the variability across time steps during inference. To address this, activation quantization is performed after weight quantization (lines 19-22) to facilitate smoother optimization and effectively minimize reconstruction error. Once sufficient optimization is achieved at τ bit-width, the transition to the second stage (for target bit-width κ) is dynamically determined using a bit-transition detection mechanism.

Momentum-based Bit Transition Detection. In PQ, the timing of bit-width transitions is crucial. A rapid transition to the target bit-width κ fails to leverage the benefits of higher bit-width τ , leading to inadequate weight perturbation reduction and generative quality degradation. Conversely, overly delayed transitions hamper optimization at the target precision κ , causing reconstruction errors. Prior work [25] introduced adaptive bit-width reductions with fixed cycles to minimize perturbation. However, the large scale and variability of DMs

Algorithm 2 Progressive Quantization (PQ)

1: **Input:** pre-trained FP model $\hat{\mathbf{x}}_\eta$ with weights η , quantization method \mathcal{Q} , target bit-widths $\{\tau, \kappa\}$ with $\tau > \kappa$, calibration dataset \mathcal{C}_{QC} , learning rate γ

2: **Output:** quantized model $\hat{\mathbf{x}}_\eta^\kappa$

3: **for** each block (or layer) $i = 1, 2, \dots, N$ **do**

4: collect calibration outputs $\hat{\mathbf{a}}_i \in \mathcal{C}_{\text{QC}}$

5: set target bit-width: $b \leftarrow \tau$

6: initialize quantized weights $\eta_i^b = \mathcal{Q}(\eta_i, b)$

7: /* weight quantization */

8: **for** each iteration $j = 1, 2, \dots$ **do**

9: quantize block outputs to b -bits: $\mathbf{a}_i^b := \mathcal{Q}(\hat{\mathbf{a}}_i, b)$

10: compute perturbation: $\Delta \mathbf{a}_i = \mathbf{a}_i^b - \hat{\mathbf{a}}_i$

11: update quantized weights using GD (6):

$$\eta_i^b \leftarrow \eta_i^b - \gamma \nabla_{\eta_i^b} \mathbb{E} \left[\Delta \mathbf{a}_i^\top \mathbf{H}^{\mathbf{a}_i} \Delta \mathbf{a}_i \right]$$

12: round weights to b -bit: $\eta_i^b \leftarrow \text{round}_b(\eta_i^b)$

13: **if** bit-transition flag in Alg. 3 **then**

14: break

15: **end if**

16: **end for**

17: **end for**

18: /* activation quantization */

19: **for** each block (or layer) $i = 1, 2, \dots, N$ **do**

20: quantize activations to b -bits: $\mathbf{a}_i^b = \mathcal{Q}(\hat{\mathbf{a}}_i, b)$

21: update target bit-width: $b \leftarrow \kappa$ and repeat

22: **end for**

Algorithm 3 Momentum-based Bit Transition Detection

1: **Input:** perturbation loss window $\mathcal{W}_{\text{pert}}$ of size W (queue), momentum coefficient β , threshold π , small constant ϵ

2: **Output:** bit-transition flag (True/False)

3: **Initialize:** perturbation loss window $\mathcal{W}_{\text{pert}} = \emptyset$, $\mathcal{G} = 0$

4: compute perturbation: $\Delta \mathbf{a}_i = \mathbf{a}_i^\tau - \hat{\mathbf{a}}_i$

5: Append to loss window: $\mathcal{W}_{\text{pert}} \leftarrow \mathcal{W}_{\text{pert}} \cup \Delta \mathbf{a}_i$

6: **if** $\mathcal{G} = 0$ **then** set $\mathcal{G} \leftarrow \Delta \mathbf{a}_i$

7: **else** update momentum: $\mathcal{G} \leftarrow \beta \cdot \mathcal{G} + (1 - \beta) \cdot \Delta \mathbf{a}_i$

8: **end if**

9: **if** $|\mathcal{W}_{\text{pert}}| = W$ **then**

10: compute average loss and momentum change rate:

$$L_{\text{avg}} \leftarrow \frac{1}{W} \sum_{l \in \mathcal{W}_{\text{pert}}} l, \quad \text{rate} \leftarrow \frac{|L_{\text{avg}} - \mathcal{G}|}{\max(L_{\text{avg}}, \epsilon)}$$

11: **if** rate $< \pi$ **then** return **True** (i.e., transition detected)

12: **end if**

13: **end if**

make frequent transitions ineffective, as they leave insufficient time for proper optimization of perturbation errors.

To address this, we propose a *momentum-based bit transition detection* to detect the optimal point of transition while using a fixed intermediate bit-width τ . This mechanism identifies steep gradients in weight perturbation loss at τ -bit model, signaling sufficient optimization and readiness to transition to

κ . The momentum \mathcal{G} , accumulates gradients to track changes in perturbation, is updated as follows:

$$\mathcal{G} \leftarrow \beta \cdot \mathcal{G} + (1 - \beta) \cdot \Delta \mathbf{a}_i, \quad (7)$$

where $\beta \in [0, 1)$ is the momentum coefficient, and $\Delta \mathbf{a}_i$ represents the change in perturbation for the i -th block or layer. When the average change rate of perturbation loss (computed within a fixed-size window) falls below a threshold π , the bit-width transitions to κ , as details are provided Alg. 3. This ensures transitions occur only when higher-bit optimization saturates, preventing premature or delayed transitions that could degrade performance.

D. Calibration-Assisted Distillation (CAD)

While diffusion distillation [11] has been proposed to accelerate inference for full-precision (FP) DMs, it struggles to preserve the student’s precision in quantized environments due to its reliance solely on a teacher-dependent inheritance structure. To address this limitation, we propose Calibration-Assisted Distillation (CAD), which minimizes errors during the distillation process of a quantized teacher model $\hat{\mathbf{x}}_\eta^\kappa$ by incorporating a dedicated calibration dataset \mathcal{C}_{DC} . CAD builds upon conventional distillation [19], which typically combines two loss terms: the first term for classification performance between the ground-truth and the student network, and the second term for the difference between the teacher and student networks. In contrast, diffusion distillation [11] employs only the second term, leading to weaker precision for the quantized student network $\hat{\mathbf{x}}_\theta^\kappa$. To overcome this, we introduce a calibration dataset \mathcal{C}_{DC} generated by the FP model as the ground-truth, enabling a direct comparison with the student.

As illustrated in Fig. 2 (right), CAD introduces a dual-objective loss function that combines knowledge distillation loss ($Loss_{\text{KD}}$) in [11] and calibration loss ($Loss_{\text{CD}}$). This ensures that the student model $\hat{\mathbf{x}}_\theta^\kappa$ inherits knowledge from the teacher $\hat{\mathbf{x}}_\eta^\kappa$ while aligning its outputs with the calibration dataset obtained from the FP model. The objective function is defined as:

$$\mathcal{L}_{\text{CAD}} = w(\lambda_t) \underbrace{\|\tilde{\mathbf{x}} - \hat{\mathbf{x}}_\theta^\kappa(\mathbf{z}_t)\|_2^2}_{Loss_{\text{KD}}} + \lambda \cdot \underbrace{\text{EM}(\mathcal{C}_{\text{DC}}, \hat{\mathbf{x}}_\theta^\kappa(\mathbf{z}_t))}_{Loss_{\text{CD}}}, \quad (8)$$

where $\tilde{\mathbf{x}}$ represents the teacher model’s output after two sampling steps and $w(\lambda_t)$ is a pre-defined coefficient function proposed by diffusion distillation that adjusts loss function weights at each time step t (see (1) and (3)). $\text{EM}(\cdot)$ denotes the Earth-Mover Distance, which measures the minimal effort required to align two distributions, making it highly sensitive to small differences, and λ is a hyperparameter to balance the contributions of $Loss_{\text{KD}}$ and $Loss_{\text{CD}}$. Note that the calibration loss $Loss_{\text{CD}}$ computes the EM distance between the student model’s output $\hat{\mathbf{x}}_\theta^\kappa(\mathbf{z}_t)$ at the current time step (e.g., $T/2$) and the FP calibration output from the corresponding time step (e.g., T). By combining two loss terms, CAD ensures both knowledge transfer from the teacher and calibration consistency with the FP model. Please refer to Alg. 4 for implementation details.

| Methods | Time Step | Bits (W/A) | LSUN-Bedrooms | | LSUN-Churches | | CelebA-HQ | | CIFAR-10 | |
|-----------------------|-----------|------------|----------------------|-----------------------|---------------------|----------------------|----------------------|----------------------|----------------------|---------------------|
| | | | FID↓ | sFID↓ | FID↓ | sFID↓ | FID↓ | sFID↓ | FID↓ | IS↑ |
| Full Prec. | 100 | 32/32 | 2.98 | 7.09 | 4.12 | 10.89 | 8.74 | 10.16 | 4.23 | 9.04 |
| Distill DM only | 50 | 32/32 | 3.07 | 7.15 | 4.26 | 11.01 | 9.01 | 10.83 | 4.28 | 9.12 |
| PTQ4DM | 100 | 8/8 | 4.75 | 9.59 | 4.80 | 13.48 | 14.42 | 15.06 | 19.59 | 9.02 |
| Q-Diff | 100 | 8/8 | 4.51 | 8.17 | 4.41 | 12.23 | 12.85 | 14.16 | 4.78 | 8.82 |
| TFMQ-DM | 100 | 8/8 | 3.14 | 7.26 | 4.01 | 10.98 | 8.91 | 10.20 | 4.24 | 9.07 |
| PTQ4DM + Bit-shrink | 100 | 8/8 | 6.45 | 10.75 | 7.68 | 15.49 | 18.12 | 19.69 | 22.37 | 8.08 |
| Q-Diff + Bit-shrink | 100 | 8/8 | 6.48 | 10.15 | 7.44 | 15.31 | 18.01 | 19.75 | 8.29 | 8.11 |
| TFMQ-DM + Bit-shrink | 100 | 8/8 | 5.95 | 10.11 | 7.25 | 14.97 | 18.43 | 18.46 | 8.62 | 7.85 |
| PTQ4DM + PQ (Ours) | 100 | 8/8 | 4.26 | 9.12 | 4.22 | 12.84 | 14.01 | 14.70 | 13.83 | 9.10 |
| Q-Diff + PQ (Ours) | 100 | 8/8 | 4.15 | 7.63 | 4.12 | 11.98 | 12.25 | 13.74 | 4.39 | 8.99 |
| TFMQ-DM + PQ (Ours) | 100 | 8/8 | 3.06 | 7.07 | 3.86 | 10.89 | 8.57 | 10.11 | 4.12 | 9.61 |
| PTQ4DM + Distill-DM. | 50 | 8/8 | 7.65 | 11.95 | 6.05 | 15.96 | 16.19 | 16.47 | 21.46 | 7.41 |
| Q-Diff + Distill-DM. | 50 | 8/8 | 6.12 | 10.75 | 5.98 | 14.85 | 14.10 | 15.76 | 5.69 | 7.12 |
| TFMQ-DM + Distill-DM. | 50 | 8/8 | 4.97 | 9.55 | 5.92 | 14.08 | 13.75 | 15.49 | 5.59 | 7.36 |
| PTQ4DM + CAD (Ours) | 50 | 8/8 | 5.82 | 10.24 | 5.21 | 13.94 | 14.68 | 15.40 | 17.65 | 9.11 |
| Q-Diff + CAD (Ours) | 50 | 8/8 | 4.67 | 8.25 | 4.54 | 12.33 | 12.73 | 14.22 | 4.60 | 9.00 |
| TFMQ-DM + CAD (Ours) | 50 | 8/8 | 3.27 | 7.36 | 4.18 | 11.12 | 9.01 | 11.46 | 4.33 | 9.21 |
| PQCAD-DM (PTQ4DM) | 50 | 8/8 | 4.56 (-0.19) | 9.40 (-0.19) | 4.61 (-0.19) | 13.12 (-0.36) | 14.24 (-0.18) | 15.03 (-0.03) | 14.12 (-5.47) | 9.05 (+0.03) |
| PQCAD-DM (Q-Diff) | 50 | 8/8 | 4.36 (-0.15) | 7.88 (-0.29) | 4.29 (-0.12) | 12.10 (-0.13) | 12.56 (-0.29) | 13.93 (-0.23) | 4.53 (-0.25) | 8.91 (+0.02) |
| PQCAD-DM (TFMQ-DM) | 50 | 8/8 | 3.10 (-0.04) | 7.12 (-0.14) | 3.92 (-0.09) | 10.94 (-0.04) | 8.65 (-0.26) | 10.15 (-0.05) | 4.19 (-0.05) | 9.53 (+0.46) |
| PTQ4DM | 100 | 4/8 | 20.72 | 54.30 | 4.97 | 14.87 | 17.08 | 17.48 | 5.14 | 8.93 |
| Q-Diff | 100 | 4/8 | 6.40 | 17.93 | 4.66 | 13.94 | 15.55 | 16.86 | 4.98 | 9.12 |
| TFMQ-DM | 100 | 4/8 | 3.68 | 7.65 | 4.14 | 11.46 | 8.76 | 10.26 | 4.78 | 9.13 |
| PQCAD-DM (PTQ4DM) | 50 | 4/8 | 20.47 (-0.25) | 39.88 (-14.42) | 4.91 (-0.06) | 14.02 (-0.85) | 16.89 (-0.19) | 17.09 (-0.39) | 4.98 (-0.16) | 9.05 (+0.12) |
| PQCAD-DM (Q-Diff) | 50 | 4/8 | 6.29 (-0.11) | 16.12 (-1.81) | 4.59 (-0.07) | 12.65 (-1.29) | 15.01 (-0.54) | 16.20 (-0.66) | 4.82 (-0.16) | 9.17 (+0.05) |
| PQCAD-DM (TFMQ-DM) | 50 | 4/8 | 3.64 (-0.04) | 7.46 (-0.19) | 3.82 (-0.32) | 11.44 (-0.02) | 8.57 (-0.19) | 10.12 (-0.14) | 4.73 (-0.05) | 9.15 (+0.02) |

TABLE I: Performance comparisons of PQCAD-DM with baseline methods across various datasets and metrics (FID, sFID, IS). Results are shown for different quantization settings (Bits (W/A)) and sampling steps (T). Improvements over baselines are highlighted in blue.

Algorithm 4 Calibration-Assisted Distillation (CAD)

- Input:** quantized teacher DM $\hat{\mathbf{x}}_{\eta}^{\kappa}$ with weights η and sampling steps T , training dataset \mathcal{D} , calibration dataset \mathcal{C}_{DC} , noise schedule factors $\{\alpha_t, \sigma_t\}_{t=0}^T$, coefficient function $w(\cdot)$, hyperparameter λ , learning rate γ
- Output:** distilled student DM $\hat{\mathbf{x}}_{\theta}^{\kappa}$ with weights θ
- initialize:** $\hat{\mathbf{x}}_{\theta}^{\kappa} = \hat{\mathbf{x}}_{\eta}^{\kappa}$ \triangleright copy student from teacher
- while** not converged **do** \triangleright distillation
- sample data and noise: $\mathbf{x} \sim \mathcal{D}$, $\epsilon \sim \mathcal{N}(\mathbf{0}, \mathbf{I})$
- sample time step $t = i/T$ with $i \sim \text{Cat}[1, 2, \dots, T]$
- add noise to data: $\mathbf{z}_t = \alpha_t \mathbf{x} + \sigma_t \epsilon$
- compute intermediate steps:

$$t' = t - 0.5/T, \quad t'' = t - 1/T$$

- perform 2 steps of DDIM sampling with $\hat{\mathbf{x}}_{\eta}^{\kappa}$:

$$\mathbf{z}_{t'} = \alpha_{t'} \hat{\mathbf{x}}_{\eta}^{\kappa}(\mathbf{z}_t) + \frac{\sigma_{t'}}{\sigma_t} (\mathbf{z}_t - \alpha_t \hat{\mathbf{x}}_{\eta}^{\kappa}(\mathbf{z}_t)),$$

$$\mathbf{z}_{t''} = \alpha_{t''} \hat{\mathbf{x}}_{\eta}^{\kappa}(\mathbf{z}_{t'}) + \frac{\sigma_{t''}}{\sigma_{t'}} (\mathbf{z}_{t'} - \alpha_{t'} \hat{\mathbf{x}}_{\eta}^{\kappa}(\mathbf{z}_{t'}))$$

- compute the teacher target: $\tilde{\mathbf{x}} = \frac{\mathbf{z}_{t''} - (\sigma_{t''}/\sigma_t)\mathbf{z}_t}{\alpha_{t''} - (\sigma_{t''}/\sigma_t)\alpha_t}$
- sample calibration data: $\mathbf{x}_t \sim \{\mathbf{x}_t^i \mid \mathbf{x}_t^i \in \mathcal{C}_{DC}\}$
- update student model via SGD with \mathcal{L}_{CAD} in (8) as:

$$\mathcal{L}_{CAD} = w(\lambda_t) \|\tilde{\mathbf{x}} - \hat{\mathbf{x}}_{\theta}^{\kappa}(\mathbf{z}_t)\|_2^2 + \lambda \cdot \text{EM}(\mathbf{x}_t, \hat{\mathbf{x}}_{\theta}^{\kappa}(\mathbf{z}_t)),$$

$$\theta \leftarrow \theta - \gamma \nabla_{\theta} \mathcal{L}_{CAD}$$

- end while**

V. EXPERIMENTS

A. Experiments Setup.

To evaluate the effectiveness of PQCAD-DM, we conducted extensive experiments across multiple generative benchmarks,

emphasizing improvements in generative performance, computational efficiency, and compression quality.

Datasets and Baselines. We evaluated PQCAD-DM on CIFAR-10 (32×32), ImageNet (64×64), CelebA-HQ and LSUN-Bedrooms/Churches (256×256 high-resolution) datasets. Two prominent diffusion model (DM) architectures, DDIM [14] and Latent Diffusion Models (LDM) [31], were employed. PQCAD-DM was implemented with SOTA quantization baselines Q: (i) PTQ4DM [9], employing block-wise reconstruction and QDrop; (ii) Q-Diff [10], using layer-wise reconstruction and split quantization; and TFMQ-DM [28], an extension of Q-Diff with temporal-aware calibration. Quantization calibration datasets \mathcal{C}_{QC} were tailored to specific methods: constructed using NDTC for PTQ4DM, and time-step specific and batch-sized sampling for Q-Diff and TFMQ-DM. Distillation calibration dataset \mathcal{C}_{DC} was created from FP models, with a size equal to the number of time steps T .

Metrics and Experimental Configurations. Generative quality is assessed using Frechet Inception Distance (FID), sliding FID (sFID), and Inception Score (IS) on 50K generated images. These images are also evaluated for downstream classification tasks (Precision, Recall, and F1 score). Experiments were conducted with various bit-widths, where Bit(W/A) denotes the precision of weights/activations. Experiments use $T = 100$ sampling steps for baselines and 50 steps for PQCAD-DM.

For progressive quantization, we set bit-width sets τ and κ to differ by a factor of two. Quantized weights are reconstructed over 20K iterations with a batch size of 32 for both DDIM and LDM. For activation quantization, PTQ4DM adopts QDrop [32], Q-Diff uses step size learning [33], and TFMQ-DM estimates activation ranges via EMA [28]. For momentum-based bit transition, we use a threshold $\pi = 0.04$, momentum coefficient $\beta = 0.9$, and $\epsilon = 1e-8$ to prevent numerical instability. The loss window size W is set to 500.



Fig. 4: 256×256 image generation results using TFMQ-DM, Q-Diff and PQCAD-DM under 4/8-bit precision.

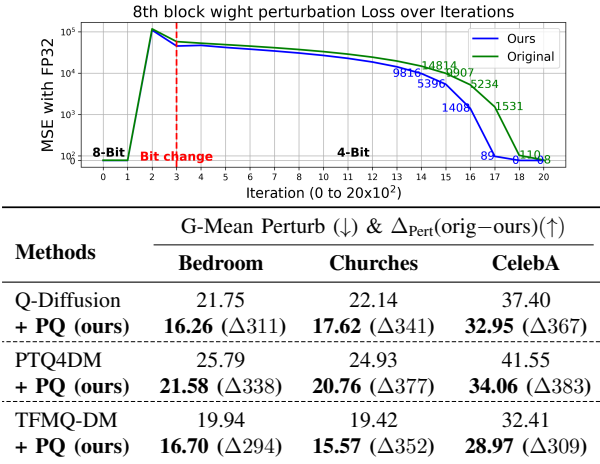


Fig. 5: (Top) Weight perturbation loss over iterations for the 8th block, comparing TFMQ-DM at 4-bit with PQCAD-DM transitioning from 8 to 4-bit. (Bottom) Geometric mean perturbation (G-Mean) and improvement (Δ_{Pert}) across methods quantized to 4/8 bits.

B. Main Results

Comparison with Baselines. As shown in Tab. I ①, PQCAD-DM demonstrates superior generative quality and computational efficiency compared to three popular quantization methods: PTQ4DM, Q-Diff, and TFMQ-DM. PQCAD-DM halves the sampling steps while maintaining or surpassing baseline performance across all datasets. For example, on CelebA-HQ dataset, PQCAD-DM with TFMQ-DM achieves an FID of 8.57 and sFID of 10.12 at 50 sampling steps, outperforming TFMQ-DM’s FID of 8.76 and sFID of 10.26 at 100 steps, and even matching the full-precision model (FID of 8.74 and sFID of 10.16). Similar improvements are observed on LSUN-Bedrooms/Churches and CIFAR-10, where PQCAD-DM consistently improves FID, sFID and IS metrics under various quantization scenarios. Notably, PQCAD-DM excels under strict compression settings, such as 4/8-bit quantization. On LSUN-Churches, it achieves an FID of 3.64 and sFID of 7.46, showcasing significant computational efficiency. Fig. 4 illustrates PQCAD-DM’s qualitative superiority, showcasing better preservation of fine-grained details and structural consistency compared to TFMQ-DM.

Impact of PQ. The effectiveness of PQ is highlighted in Tab. I ②. Momentum-based bit transitions in PQ consistently

outperform frequent bit-shrinking methods [25]. For instance, on CIFAR-10, PQ with 8/8-bit PTQ4DM reduces the FID from 19.59 to 13.83 and improves IS from 9.02 to 9.10 compared to PTQ4DM alone. PQ effectively minimizes perturbations at higher bit-widths (τ) and transitions smoothly to lower bit-widths (κ), as indicated by the geometric mean perturbation improvement (Δ_{Pert}) across datasets (see Fig. 5 (Bottom)). Additionally, PQCAD-DM’s adaptive bit transition mechanism significantly reduces perturbations after transitioning, as seen in Fig. 5 (Top), where the optimization process accelerates across all blocks due to the stimulating effect of momentum-based transitions.

Impact of CAD. Tab. I ③ highlights CAD’s ability to mitigate distillation-induced errors. CAD significantly improves FID and sFID metrics compared to traditional Distill-DM [11]. For example, on LSUN-Churches, CAD applied to Q-Diff reduces an FID from 5.98 to 4.54 and sFID from 14.85 to 12.33, compared to Q-Diff with Distill-DM. Even with halved sampling steps, PQCAD-DM achieves performance comparable to non-distilled Q-Diff (FID 4.41 and sFID 12.23). Similar trends are observed across other base methods, underscoring CAD’s robustness in maintaining generative quality under reduced precision.

Computational Efficiency Analysis. We evaluate the model size, inference time, throughput, and maximum batch size and bit-operations (GBOPs) across multiple datasets in Table II. All models operate under identical GPU A6000 memory constraints. GBOPs are computed as the total bit-level operations per forward pass, considering both weights and activations. PQCAD-DM consistently achieves faster inference, higher throughput, and larger batch sizes than both Q-Diff and TFMQ-DM. For instance, on LSUN-Bedroom, PQCAD-DM runs 1.6 \times faster than Q-Diff (204.65 vs. 340.11 minutes) while achieving double the efficiency in terms of GBOPs (3,240 vs. 6,480). Similar trends are observed across other datasets. By aggressively reducing bit-widths without degrading generation quality, PQCAD-DM significantly lowers computational overhead, enabling superior hardware utilization in resource-constrained environments.

C. Ablation Study

Impact of C_{DC} Composition. We assessed the effect of stochastic versus deterministic sampling for constructing the

| Dataset | Method | Model Size (MB) | Time (min) | Throughput (img/sec) | Max Batch Size | GBOPs |
|---------------|-----------------|-----------------|---------------|----------------------|----------------|--------------|
| LSUN-Churches | FP32 | 1,179.9 | 5,655.7 | 0.013 | 1.0× | 22,170 |
| | Q-Diff | 147.5 | 342.15 | 0.224 | 2.6× | 1,340 |
| | TFMQ-DM | 147.5 | 315.43 | 0.264 | 3.2× | 1,340 |
| | PQCAD-DM | 147.5 | 206.52 | 0.440 | 3.2× | 670 |
| LSUN-Bedroom | FP32 | 1,096.2 | 5,620.33 | 0.013 | 1.0× | 107,170 |
| | Q-Diff | 137 | 340.11 | 0.226 | 2.4× | 6,480 |
| | TFMQ-DM | 137 | 312.39 | 0.267 | 2.9× | 6,480 |
| | PQCAD-DM | 137 | 204.65 | 0.446 | 2.9× | 3,240 |
| CelebA | FP32 | 1,096.2 | 5,571.52 | 0.014 | 1.0× | 107,170 |
| | Q-Diff | 137 | 336.97 | 0.232 | 2.4× | 6,480 |
| | TFMQ-DM | 137 | 308.45 | 0.271 | 2.9× | 6,480 |
| | PQCAD-DM | 137 | 202.16 | 0.454 | 2.9× | 3,240 |
| CIFAR-10 | FP32 | 143.2 | 505.82 | 0.164 | 1.0× | 6,597 |
| | Q-Diff | 17.9 | 30.60 | 2.723 | 2.6× | 399 |
| | TFMQ-DM | 17.9 | 27.01 | 3.086 | 3.0× | 399 |
| | PQCAD-DM | 17.9 | 17.44 | 4.790 | 3.0× | 199.5 |

TABLE II: Comparison of model size, inference time, throughput (images/sec), max batch size, and GBOPs (bit-operations) for 4/8-bit 5,000 samples across datasets. PQCAD-DM demonstrates enhanced performance and computational efficiency over TFMQ-DM and Q-Diff.

| Base Method | Collection | P (↑) | R (↑) | F1 (↑) | IS (↑) / FID (↓) |
|-------------|-------------------|---------------|---------------|---------------|--------------------|
| ImageNet | Deterministic | 0.5789 | 0.6014 | 0.5900 | 15.41/24.45 |
| PTQ4DM | Stochastic | 0.6175 | 0.6201 | 0.6188 | 15.60/22.78 |
| ImageNet | Deterministic | 0.6023 | 0.6189 | 0.6105 | 15.38/12.05 |
| Q-Diff | Stochastic | 0.6345 | 0.6372 | 0.6358 | 15.91/10.56 |
| ImageNet | Deterministic | 0.6178 | 0.6285 | 0.6225 | 15.78/10.45 |
| TFMQ-DM | Stochastic | 0.6409 | 0.6444 | 0.6423 | 16.07/9.89 |

TABLE III: Classification accuracy (P: Precision, R: Recall, F1) and image generation quality (IS, FID) for different calibration data collection methods (Deterministic vs. Stochastic) across PTQ4DM, Q-Diff and TFMQ-DM with 4/8-bit quantization on ImageNet DDIM.

calibration dataset \mathcal{C}_{DC} in CAD phase. Stochastic sampling introduces noise variability, avoiding overfitting and improving generalization, as discussed in Sec. IV-B. The downstream task involved classification accuracy on ImageNet using 10K generated samples evaluated with an Inception v3 model. As shown in Tab. III, stochastic sampling outperforms deterministic sampling with up to 4.88% higher F1 scores, demonstrating its efficacy in preventing biased generation.

Distance Measures in $Loss_{CD}$. We analyzed the performance of various distance measures for $Loss_{CD}$ in (8). Cosine similarity underperformed due to its inability to measure probabilistic distributions. In contrast, KL and JSD divergence metrics demonstrated slight improvements but were less effective in handling non-overlapping distributions. The Earth-Mover distance (EM) provided the most stable and meaningful measures of similarity, resulting in significant improvements in generative quality. As shown in Tab. IV, applying EM distance reduced FID and sFID by 6.69 and 10.06, respectively, when using TFMQ-DM as a base method for quantization. We further validate this observation by visualizing the evolution of each metric during distillation (Fig. 6). Cosine similarity failed to capture distributional changes due to its directional nature, while KL and JSD showed only modest sensitivity. EM distance, however, yielded clear convergence signals, supporting its effectiveness in aligning distributions and enhancing generation quality.

| CAD Methods | Base Method | Bits (W/A) | FID↓ | sFID↓ |
|--------------------------|-------------|------------|---------------------|---------------------|
| Only $Loss_{KD}$ | Full Prec. | 32/32 | 3.07 | 7.15 |
| Only $Loss_{KD}$ | Q-Diff | 8/8 | 6.12 | 10.75 |
| | TFMQ-DM | 8/8 | 4.97 | 9.55 |
| + $Loss_{CD}$ (Cos-Dist) | Q-Diff | 8/8 | 8.95 | 12.56 |
| | TFMQ-DM | 8/8 | 6.47 | 11.45 |
| + $Loss_{CD}$ (KL-Div) | Q-Diff | 8/8 | 5.75 | 9.83 |
| | TFMQ-DM | 8/8 | 4.73 | 9.26 |
| + $Loss_{CD}$ (JSD-Div) | Q-Diff | 8/8 | 5.18 | 9.49 |
| | TFMQ-DM | 8/8 | 4.59 | 9.04 |
| + $Loss_{CD}$ (EM-Dist) | Q-Diff | 8/8 | 4.36 (-1.76) | 7.88 (-2.87) |
| | TFMQ-DM | 8/8 | 3.10 (-1.87) | 7.12 (-2.43) |

TABLE IV: Performance of CAD with different $Loss_{CD}$ settings using teacher model quantized by Q-Diff/TFMQ-DM on LSUN-Bedrooms LDM. Blue indicates improvements relative to baseline.

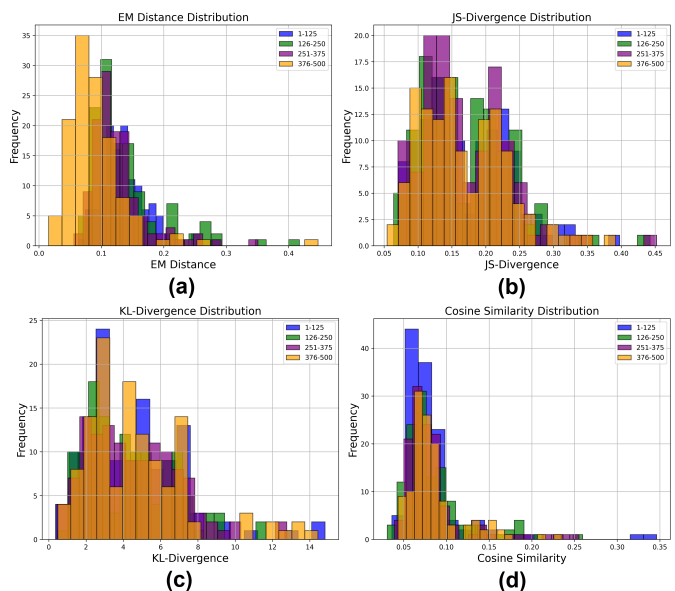


Fig. 6: Changes in L_{CD} during the 500-step distillation process, plotted with respect to distance. Colors represent different distillation stages. Results are based on unconditional image generation with a 256×256 LSUN-Bedrooms LDM at 8/8-bit 100 sampling steps.

VI. DISCUSSION AND FUTURE WORK

VII. CONCLUSION

In this work, we introduced PQCAD-DM, a hybrid framework combining progressive quantization and calibration-assisted distillation to compress diffusion models effectively. By leveraging dual calibration datasets, PQ and CAD, our method minimizes error accumulation and balances computational efficiency (halving inference time) with generative performance. Experimental results demonstrate that PQCAD-DM achieves significant reductions in memory and sampling steps while maintaining competitive generative quality across diverse datasets and architectures. Our approach highlights the importance of tailored calibration and sequential optimization for compressing diffusion models, paving the way for future research in efficient activation quantization.

REFERENCES

- [1] Jonathan Ho, Ajay Jain, and Pieter Abbeel, “Denoising diffusion probabilistic models,” *Advances in neural information processing systems*, vol. 33, pp. 6840–6851, 2020.
- [2] Ian Goodfellow, Jean Pouget-Abadie, Mehdi Mirza, Bing Xu, David Warde-Farley, Sherjil Ozair, Aaron Courville, and Yoshua Bengio, “Generative adversarial networks,” *Communications of the ACM*, vol. 63, no. 11, pp. 139–144, 2020.
- [3] Prafulla Dhariwal and Alexander Nichol, “Diffusion models beat gans on image synthesis,” *Advances in neural information processing systems*, vol. 34, pp. 8780–8794, 2021.
- [4] Diederik P Kingma, “Auto-encoding variational bayes,” *arXiv preprint arXiv:1312.6114*, 2013.
- [5] Yang Song, Jascha Sohl-Dickstein, Diederik P Kingma, Abhishek Kumar, Stefano Ermon, and Ben Poole, “Score-based generative modeling through stochastic differential equations,” *arXiv preprint arXiv:2011.13456*, 2020.
- [6] Andreas Lugmayr, Martin Danelljan, Andres Romero, Fisher Yu, Radu Timofte, and Luc Van Gool, “Repaint: Inpainting using denoising diffusion probabilistic models,” in *Proceedings of the IEEE/CVF conference on computer vision and pattern recognition*, 2022, pp. 11461–11471.
- [7] Chenhao Niu, Yang Song, Jiaming Song, Shengjia Zhao, Aditya Grover, and Stefano Ermon, “Permutation invariant graph generation via score-based generative modeling,” in *International Conference on Artificial Intelligence and Statistics*. PMLR, 2020, pp. 4474–4484.
- [8] Minkai Xu, Lantao Yu, Yang Song, Chence Shi, Stefano Ermon, and Jian Tang, “Geodiff: A geometric diffusion model for molecular conformation generation,” *arXiv preprint arXiv:2203.02923*, 2022.
- [9] Yuzhang Shang, Zhihang Yuan, Bin Xie, Bingzhe Wu, and Yan Yan, “Post-training quantization on diffusion models,” in *Proceedings of the IEEE/CVF conference on computer vision and pattern recognition*, 2023, pp. 1972–1981.
- [10] Xiuyu Li, Yijiang Liu, Long Lian, Huanrui Yang, Zhen Dong, Daniel Kang, Shanghang Zhang, and Kurt Keutzer, “Q-diffusion: Quantizing diffusion models,” in *Proceedings of the IEEE/CVF International Conference on Computer Vision*, 2023, pp. 17535–17545.
- [11] Tim Salimans and Jonathan Ho, “Progressive distillation for fast sampling of diffusion models,” *arXiv preprint arXiv:2202.00512*, 2022.
- [12] Chenlin Meng, Robin Rombach, Ruiqi Gao, Diederik Kingma, Stefano Ermon, Jonathan Ho, and Tim Salimans, “On distillation of guided diffusion models,” in *Proceedings of the IEEE/CVF Conference on Computer Vision and Pattern Recognition*, 2023, pp. 14297–14306.
- [13] Jonathan Ho, Ajay Jain, and Pieter Abbeel, “Denoising diffusion probabilistic models,” *Advances in neural information processing systems*, vol. 33, pp. 6840–6851, 2020.
- [14] Jiaming Song, Chenlin Meng, and Stefano Ermon, “Denoising diffusion implicit models,” *arXiv preprint arXiv:2010.02502*, 2020.
- [15] Alexander Quinn Nichol and Prafulla Dhariwal, “Improved denoising diffusion probabilistic models,” in *International conference on machine learning*. PMLR, 2021, pp. 8162–8171.
- [16] Alexander Quinn Nichol and Prafulla Dhariwal, “Improved denoising diffusion probabilistic models,” in *International conference on machine learning*. PMLR, 2021, pp. 8162–8171.
- [17] Gongfan Fang, Xinyin Ma, and Xinchao Wang, “Structural pruning for diffusion models,” *Advances in Neural Information Processing Systems*, vol. 36, 2024.
- [18] Thibault Castells, Hyoung-Kyu Song, Bo-Kyeong Kim, and Shinkook Choi, “Ld-pruner: Efficient pruning of latent diffusion models using task-agnostic insights,” in *Proceedings of the IEEE/CVF Conference on Computer Vision and Pattern Recognition*, 2024, pp. 821–830.
- [19] Geoffrey Hinton, “Distilling the knowledge in a neural network,” *arXiv preprint arXiv:1503.02531*, 2015.
- [20] Bohan Zhuang, Chunhua Shen, Mingkui Tan, Lingqiao Liu, and Ian Reid, “Towards effective low-bitwidth convolutional neural networks,” in *Proceedings of the IEEE conference on computer vision and pattern recognition*, 2018, pp. 7920–7928.
- [21] Bohan Zhuang, Chunhua Shen, Mingkui Tan, Lingqiao Liu, Ian Reid, and Chunhua Shen, “Effective training of convolutional neural networks with low-bitwidth weights and activations,” *IEEE Transactions on Pattern Analysis and Machine Intelligence*, vol. 44, no. 10, pp. 6140–6152, 2021.
- [22] Zhongnan Qu, Zimu Zhou, Yun Cheng, and Lothar Thiele, “Adaptive loss-aware quantization for multi-bit networks,” in *Proceedings of the IEEE/CVF Conference on Computer Vision and Pattern Recognition*, 2020, pp. 7988–7997.
- [23] HyunJin Kim, Jungwoo Shin, and Alberto A Del Barrio, “Ctmq: Cyclic training of convolutional neural networks with multiple quantization steps,” *arXiv preprint arXiv:2206.12794*, 2022.
- [24] Sangil Jung, Changyong Son, Seohyung Lee, Jinwoo Son, Jae-Joon Han, Youngjun Kwak, Sung Ju Hwang, and Changkyu Choi, “Learning to quantize deep networks by optimizing quantization intervals with task loss,” in *Proceedings of the IEEE/CVF conference on computer vision and pattern recognition*, 2019, pp. 4350–4359.
- [25] Chen Lin, Bo Peng, Zheyang Li, Wenming Tan, Ye Ren, Jun Xiao, and Shiliang Pu, “Bit-shrinking: Limiting instantaneous sharpness for improving post-training quantization,” in *Proceedings of the IEEE/CVF Conference on Computer Vision and Pattern Recognition*, 2023, pp. 16196–16205.
- [26] Diederik Kingma, Tim Salimans, Ben Poole, and Jonathan Ho, “Variational diffusion models,” *Advances in neural information processing systems*, vol. 34, pp. 21696–21707, 2021.
- [27] Junhyuk So, Jungwon Lee, Daehyun Ahn, Hyungjun Kim, and Eunhyeok Park, “Temporal dynamic quantization for diffusion models,” *Advances in Neural Information Processing Systems*, vol. 36, 2024.
- [28] Yushi Huang, Ruihao Gong, Jing Liu, Tianlong Chen, and Xianglong Liu, “Tfmq-dm: Temporal feature maintenance quantization for diffusion models,” in *Proceedings of the IEEE/CVF Conference on Computer Vision and Pattern Recognition*, 2024, pp. 7362–7371.
- [29] Markus Nagel, Rana Ali Amjad, Mart Van Baalen, Christos Louizos, and Tijmen Blankevoort, “Up or down? adaptive rounding for post-training quantization,” in *International Conference on Machine Learning*. PMLR, 2020, pp. 7197–7206.
- [30] Yuhang Li, Ruihao Gong, Xu Tan, Yang Yang, Peng Hu, Qi Zhang, Fengwei Yu, Wei Wang, and Shi Gu, “Breq: Pushing the limit of post-training quantization by block reconstruction,” *arXiv preprint arXiv:2102.05426*, 2021.
- [31] Robin Rombach, Andreas Blattmann, Dominik Lorenz, Patrick Esser, and Björn Ommer, “High-resolution image synthesis with latent diffusion models,” in *Proceedings of the IEEE/CVF conference on computer vision and pattern recognition*, 2022, pp. 10684–10695.
- [32] Xiuying Wei, Ruihao Gong, Yuhang Li, Xianglong Liu, and Fengwei Yu, “Qdrop: Randomly dropping quantization for extremely low-bit post-training quantization,” *arXiv preprint arXiv:2203.05740*, 2022.
- [33] Steven K Esser, Jeffrey L McKinstry, Deepika Bablani, Rathinakumar Appuswamy, and Dharmendra S Modha, “Learned step size quantization,” *arXiv preprint arXiv:1902.08153*, 2019.



Beomseok Ko (Student Member, IEEE) received the B.S. degree in Information and Communication Engineering from Dongguk University, Seoul, South Korea, in 2023. He is currently pursuing the M.S. degree in Computer Science and Artificial Intelligence at Dongguk University. His research interests include model compression and the application of diffusion models.



Hyeryung Jang (Member, IEEE) received the B.S., M.S., and Ph.D. degrees from the School of Electrical Engineering, Korea Advanced Institute of Science and Technology (KAIST), Daejeon, South Korea, in 2010, 2012, and 2017, respectively. From 2018 to 2021, she was a Research Associate with the Department of Informatics, King's College London, London, U.K. She is currently an Assistant Professor with the Division of Computer Science and Artificial Intelligence, Dongguk University, Seoul, South Korea. Her research interests include learning and inference of probabilistic graphical models, machine learning on networked systems, wireless communications, and neuromorphic computing.